Journal of Asian Earth Sciences 147 (2017) 210–221

Contents lists available at ScienceDirect

Journal of Asian Earth Sciences

journal homepage: www.elsevier.com/locate/jseaes

Full length article

# 3-D magnetotelluric imaging of the Phayao Fault Zone, Northern Thailand: Evidence for saline fluid in the source region of the 2014 Chiang Rai earthquake

Songkhun Boonchaisuk[a], Sutthipong Noisagool[b,e], Puwis Amatyakul[b], Tawat Rung-Arunwan[c], Chatchai Vachiratienchai[c], Weerachai Siripunvaraporn[b,d,*]

[a] Geoscience Program, Mahidol University, Kanchanaburi Campus, Saiyok, Kanchanaburi, Thailand
[b] Department of Physics, Faculty of Science, Mahidol University, 272 Rama 6 Road, Rachatawee, Bangkok, Thailand
[c] Curl-E Geophysics Co., Ltd., 85/87 Nantawan Village, Uttayan-Aksa Road, Salaya, Phutthamonthon, Nakornpathom 73170, Thailand
[d] ThEP Center, Commission on Higher Education, 328, Si Ayutthaya Road, Rachatawee, Bangkok, Thailand
[e] Earthquake Research Institute, University of Tokyo, 1-1-1 Yayoi, Bunkyo-ku, Tokyo, Japan

A R T I C L E I N F O

*Keywords:*
Magnetotelluric
Northern Thailand
Earthquake
Fluid
Phayao Fault Zone

A B S T R A C T

Seismicity in Thailand had been relatively low for decades prior to the Mw 6.5 earthquake of 5 May 2014 which came as a surprise and was followed by thousands of aftershocks. Most of the epicenters were located in the transition region between the Mae Lao Segment (MLS) and the Pan Segment (PS) of the Phayao Fault Zone (PFZ). We conducted a 3-D magnetotelluric (MT) survey (31 sites) to image the deep PFZ structure. The shallow 3-D resistivity structure matches very well with the surface geology, while the deeper structures disclose many interesting resistive and conductive anomalies. However, the most interesting feature of this study is the large conductive anomaly (ML) located at a depth of 4 km to the mid-crust beneath the MLS near the seismogenic zone. Our current hypothesis is that the ML conductor has a highly interconnected aqueous fluid content and also plays crucial role in the earthquake sequence of the 5 May 2014 event. As our previous seismic waveform study revealed that the MLS has a relatively high fault plane instability, the fluid within the fractured fault would further reduce the fault strength. The accumulated pre-existing tectonic stress from the north can therefore overcome the maximum frictional strength of the MLS, and hence cause it to slip and produce the main shock. With the local structural heterogeneities and fluid in the fractured fault zones, the aftershocks then occurred on both the PS and MLS. This is in contrast to the Mae Chan Fault Zone (MCFZ) in the north which many scientists expected to generate a larger magnitude earthquake than any other faults. Since instrumental record, it has only generated a few Mw 4 earthquakes. Some of our MT stations were located within the MCFZ. However, there is no deep conductor as the conductor lies beneath the MLS. A lack of interconnected fluid within the deep fault beneath the MCFZ might be one of the reasons for the lower seismic activity from the MCFZ. Other geophysical methods, such as seismic tomography, are necessary in order to confirm the presence of the fluid beneath the MLS and also the lack of a deep conductor beneath the MCFZ.

## 1. Introduction

Most of the seismicity in Thailand is localized in the north as there are many fault zones that cut through the region (Fig. 1a). The number and magnitude of earthquakes is generally lower than neighboring countries like Myanmar. Nevertheless, an unexpected moderate earthquake occurred on 5 May 2014 in Pan District, Chiang Rai province, northern Thailand (Fig. 1a and b) with thousands of aftershocks (Fig. 1b). The local magnitude (Ml) of the main shock was reported as 6.3 by the Thai Meteorological Department (TMD) with a hypocenter depth of 7 km, but later regional moment tensor inversion studies by Noisagool et al. (2016) suggested Mw 6.5 with a depth of 14 km. The main event was the largest earthquake in Thailand since the installation of the seismometer in 1974. The epicenters of the main shock and aftershocks were mostly in the Phayao Fault Zone (PFZ, Fig. 1b) which runs from south to north and is clearly separated into three major segments (Fig. 1b; Uttamo et al., 2003; DMR, 2007, 2014). The two segments involved with the recent events are the left–lateral strike–slip Mae Lao Segment (MLS) and the right lateral strike–slip Pan Segment (PS) (Fig. 1b). Interestingly, most of the epicenters are in the transition

* Corresponding author at: Department of Physics, Faculty of Science, Mahidol University, 272 Rama 6 Road, Rachatawee, Bangkok, Thailand.
*E-mail address:* wsiripun@gmail.com (W. Siripunvaraporn).

http://dx.doi.org/10.1016/j.jseaes.2017.07.034
Received 10 February 2017; Received in revised form 13 July 2017; Accepted 18 July 2017
Available online 20 July 2017
1367-9120/ 

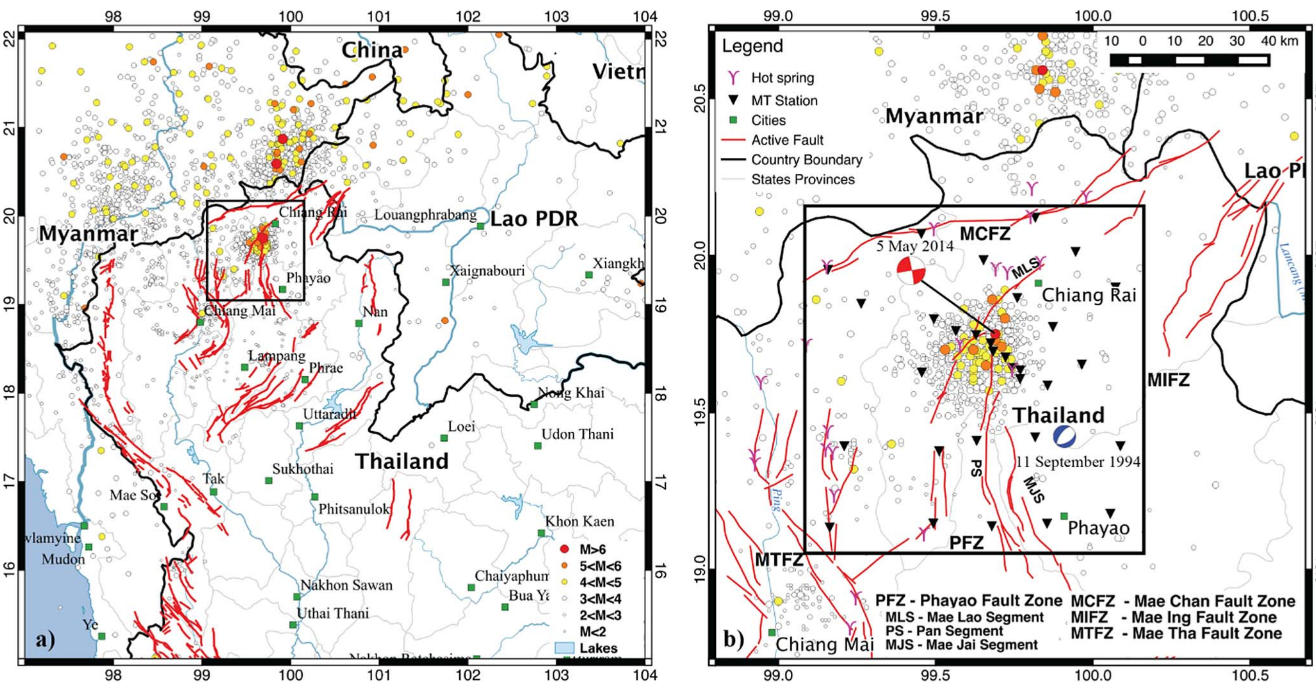


**Fig. 1.** (a) Northern Thailand and its neighboring countries with fault traces (red solid line) and seismicity from the TMD (from January 2007 – October 2016). (b) shows the study area in more detail. Triangles are the locations of the MT survey. Focal mechanisms of the 5 May 2014 (red) and 11 September 1994 (blue) are derived from Noisagool et al. (2016) and ISC (2012), respectively. The rectangles in (a) and (b) show the study area. PFZ is the Phayao Fault Zone divided into three segments, PS: Pan Segment, MLS: Mae Lao Segment and MJS: Mae Jai Segment. Legends are displayed inside the Figure. (For interpretation of the references to color in this figure legend, the reader is referred to the web version of this article.)

area between the MLS and the PS (Fig. 1b). The focal mechanisms (Noisagool et al., 2016) of most events (Ml > 4) indicate strike–slip motions in agreement with the characteristics of these fault segments.

It is interesting that the second largest recent earthquake in northern Thailand (Mw 5.2, 15 km depth, on 11 September 1994; USGS) also occurred in the PFZ (Fig. 1b). The focal mechanism of this earthquake was the normal motion (ISC, 2012; Fig. 1b). However, Noisagool et al. (2016) pointed out that its focal mechanism should be similar to the main event of the 5 May 2014. In fact, its epicenter is still in doubt as in 1994 there were no seismometers installed nearby. Since the PFZ is classified as a tentatively active fault (Charusiri et al., 1999) due to the lack of the data, even with the 1994 event (M5) and a few M4 events between 1994 and 2014 in this area, no scientists expected the PFZ to have enough energy to rupture and produce a Mw 6.5 earthquake so soon. This might be because of its very slow slip rate of about 0.1 mm/yr (Fenton et al., 2003), and relatively short length (45 km). In addition, Noisagool et al. (2016) has suggested a very crucial point about the regional stress and the fault plane instability revealed from the inversion of derived focal mechanisms from the 5 May 2014 earthquake sequences. They found that the Mae Lao Segment (MLS) has a higher shear stress than the other segments of the PFZ. With the stress from the north (≈N18E; Noisagool et al., 2016), the MLS is likely to be the fault that produced the main shock. Its movement has induced the Pan Segment (PS) which has a lower shear stress to slip. Noisagool et al. (2016) showed that there were mixtures of all three kinds of focal mechanisms: strike–slip, normal, and thrust motions. These mixed mechanisms result from the motions of both the MLS and PS and the structural heterogeneities between them.

In contrast to the PFZ, the east-trending Mae Chan Fault Zone (MCFZ, Fig. 1a) in the north of the PFZ has a slightly faster slip rate and is longer. It was classified as an active fault in the study of Charusiri et al. (1999). Most of the scientists then believed that the MCFZ would be the fault that produces large events based on its paleo-seismicity (Nutalaya et al., 1985; Charusiri et al., 2000; Fenton et al., 2003). This has led to many geological and geophysical studies on the MCFZ (e.g., Wood, 1995, 2001; Hinthong, 1995; Rymer et al., 1997; Kosuwan et al., 1998, 2000, 2003; Kosuwan and Lumjuan, 1999; Fenton et al., 2003; Wood et al., 2004, 2015; Phodee et al., 2014) in the past decades and little attention on the PFZ. In the end, only a few M4 earthquakes occurred in the MCFZ since the installation of first seismometer. With the accumulated tectonic stress coming from the north to both faults, this leads to the intriguing question of why the PFZ slipped instead of the MCFZ. Answers probably lie in the characteristics of these two faults, e.g. the fault plane, the frictional coefficient, and the interconnected fluid in the fault.

The occurrence of the largest earthquake in Thailand history on the PFZ is a good reason to conduct geological and geophysical investigations to probe the characteristic of the PFZ. One of the geophysical methods conducted worldwide is the magnetotelluric (MT) method. A magnetotelluric survey yields the resistivity structure which can be used to image faults and to study the fault properties and characteristics and its relation with earthquakes (Bedrosian et al., 2002; Becken and Ritter, 2012; Rao et al., 2004; Patro et al., 2005; Wannamaker et al., 2014; among many others). In many regions around the world, MT results reveal that high conductivity anomalies are often associated with the faults and seismicity of the region. In the San Andrea Fault, seismicity along each fault segment was linked to resistivity anomalies probed by MT surveys (Bedrosian et al., 2002, 2004; Unsworth and Bedrosian, 2004a, 2004b; Becken and Ritter, 2012). For the creeping segment of the fault, the high conductivity zone was observed within the fault indicating the presence of saline fluid. In contrast, in the locked fault segment, there was no high conductivity zone within the fractured fault. In the tectonic studies of the Central Indian Tectonic Zone, many conductors were found at different depths, e.g., from upper crust to mid-crust, and/or from mid- to lower crust, in association with the faults where seismicity also took place (e.g., Rao et al., 2004; Patro et al., 2005; Naganjaneyulu and Santosh, 2010; Abdul Azeez et al., 2013). Their interpretations of the low resistivity bodies were mainly based on either the mafic magmatic underplating and/or the presence of the aqueous fluid either in the fractures or intruding from the deep. In the Cascadia subduction system, USA (Wannamaker et al., 2014), the relatively high resistivity anomalies were interpreted as a lack of fluid and sediment indicating a plate locking zone, while the low resistivity anomalies were associated with the no plate lock zone implying with the presence of shallow sediment, and the fluid at great depth. In an arc-continent collision of Taiwan, Bertrand et al. (2012) found conductive zones at great depth and these have some relationship with the crustal seismicity. They interpreted the low resistivity zones as the interconnected saline fluid. A deep crustal conductor associated with the fluid was also observed in the New Zealand Southern Alps (Wannamaker et al., 2002) and in Japan (Mitsuhata et al., 2001; Ogawa and Honkura, 2004). The low resistivity anomalies were also found to be related to the low velocity zone in the lower crust beneath the Tangshan area indicating the existence of fluids which help to weaken the upper and middle crustal seismogenic layers and so cause large earthquakes (Wang et al., 2013). Similar scenarios were also found in the 1995 Kobe earthquake, Japan (Zhao et al., 1996), the 2001 Bhuj earthquake, India (Mishra and Zhao, 2003), the 2000 western Tottori earthquake, western Japan (Zhao et al., 2004) and the 2008 Iwate-Miyagi inland earthquake, Japan (Ichihara et al., 2011), among many others. With the correlation of low velocity and low resistivity, one of the explanations for the earthquake occurrence in these regions is the crustal heterogeneities, rather than just the stress condition alone (Zhao et al., 1996, 2004; Mishra and Zhao, 2003; Wang et al., 2013)

Many of these studies have shown the importance of MT method for studying fault zones and earthquake mechanisms. Here, to study the characteristic of the PFZ, we conducted a 3-D MT survey covering the PFZ with more stations in the region where the Pan Segment intersects the Mae Lao Segment which is the area where most of the epicenters were located. In the absence of any geological and geophysical studies, our resistivity model obtained from the MT survey is therefore the first providing detailed information in the region around the PFZ.

## 2. Regional geologic framework of the Phayao Fault Zone and Northern Thailand

The tectonic setting and the regional geologic map around the Phayao Fault Zone (PFZ) are shown in Fig. 2a and b, respectively. According to the tectono-stratigraphic zone (Metcalfe, 2013; Morley et al., 2011; DMR, 2014), the tectonics of the northern Thailand is divided into the Inthanon zone on the west (west of the Mae Tha Fault Zone, MTFZ, in Fig. 2a), the north – south trend Sukhothai fold belt in the center which covers most of our study area (Fig. 2a), and the Indochina terrane on the east (east of the Nan province in Fig. 2a) which is mostly outside our study area. The Inthanon zone which is part of the larger Shibumau terrane (Metcalfe, 1997) that collided with the Indochina terrane during the Permian and Triassic comprises mainly of the high grade metamorphic rocks and the igneous intrusion overlain by the Upper Paleozoic rocks. The Sukhothai fold belt, considered as the magmatic arc developed along the margin of the Indochina Terrane (Sone and Metcalfe, 2008; Sone et al., 2012), is underlain by the Paleozoic and Mesozoic sedimentary rocks and the volcanic rocks, intruded by the Triassic S-type granite of the Central Granitoid Belt (Charusiri et al., 1993). The folds and the strike-slip faults found in the Sukhothai fold belt is mostly associated with the collision of the Indian and Eurasian plates during the Cenozoic.

There are three major active fault zones in the northern Sukhothai fold belt: the Mae Chan Fault Zone (MCFZ), the Phayao Fault Zone (PFZ), and the Mae Tha Fault Zone (MTFZ) as shown in Figs. 1b and 2b. Unlike the orientations of the other fault zones, the left–lateral strike–slip MCFZ cuts almost east to west across the Triassic granite in northern Thailand from the Thai – Lao border in the east to terminate in the Fang basin (Fig. 2b) for a total length of around 185 km (Morley et al., 2011). Its slip rate is between 0.3 and 3 mm/yr (Fenton et al., 2003). It almost embraces one side of the 50 km long Fang basin (Fig. 2b). On the southwest of the study area, the Mae Tha Fault Zone (MTFZ) is another zone with high seismicity ( < M4) in recent years. Its orientation is N – S trending in the north but gradually forms an arcuate trace about 140 km long (Morley et al., 2011) and is convex toward the Chiang Mai basin (Fig. 1a). Interestingly, some geologists have documented the MTFZ as a strike – slip fault while some regard it as a thrust with a low dip angle (Wood and Singharajwarapan, 2014).

The Phayao Fault Zone (PFZ) which is the main focus of our study here runs from south to north. It is separated into three major segments (Figs. 1b and 2b; Uttamo et al., 2003; DMR, 2007; and DMR, 2014) with similar lengths of 50 km. In the south, the Mae Jai Segment (MJS) is oriented in the NNW – SSE trending and was classified as a normal fault by Uttamo et al. (2003). West of the MJS but slightly north is the Pan Segment (PS) which is a right lateral strike – slip fault running in an almost N – S direction. The northern end of the PS almost intersects with the NE – SW trending left lateral strike – slip Mae Lao Segment (MLS) which is the third segment of the PFZ. The transition zone between the PS and MLS is the epicenters of the 5 May 2014 events (Fig. 1b). On the west of the PFZ, the Triassic granite (Tgr) and the Carboniferous sandstone and shale (C) are aligned in the north – south direction parallel to the fault (Fig. 2b). Both are overlain by the Quaternary NNE – SSW Fang basin in the north and the Chiang Mai basin in the southwest (Fig. 2b). The surface geology of the PFZ is a mix of the Quaternary alluvial deposits (Qa), Triassic biotite granite (Tgr), and Silurian/Devonian meta-sediments and volcanic rocks (SD). The eastern side of the PFZ is mostly overlain by Quaternary sediments (Qa) on top of the Mesozoic non marine sedimentary rock (JK). The Mesozoic marine and the extrusive rocks are found to be aligned in the NE – SW and parallel to the Mae Lao segment and the MCFZ in the north east of the study area.

These three major faults (MCFZ, MTFZ and PFZ) have produced many hot springs along their surface traces. The prominent hot springs (Fig. 2) are the Mae Chan hot spring (Amatyakul et al., 2015) located at almost the center of the MCFZ, the Fang hot spring (Amatyakul et al., 2016) located at the west end of the MCFZ near the Fang basin, the mid-temperature Huai Sai Khao hot spring of the PFZ (Fig. 2b), and also many hot springs along the MTFZ.

## 3. Magnetotelluric survey and the three-dimensional inversion

In November 2015, 29 MT stations were deployed covering a 140 km × 140 km area (Fig. 1b and Fig. 2) to ensure that the MT technique can "image" the near surface down to the lower crust. Uniform coverage of the stations is impossible as some of the land was not accessible due to lack of navigable terrain and/or permission from the owner. Most of the MT sites were above sedimentary rocks (Fig. 2b) in rice and corn farms. Only a few sites were placed over the granitic rocks. The main interest of this study is the junction of the PFZ between the PS and the MLS where the epicenters of the 5 May 2014 and its aftershocks were located. Many MT stations were installed in the vicinity of these segments. Many sites were also located outside to constrain the resistivity within the area of interest. In addition to these 29 newly deployed stations, two stations from previous geothermal experiments, one from Fang hot spring area (Amatyakul et al., 2016) and another from Mae Chan hot spring area (Amatyakul et al., 2015), were also incorporated bringing the total to 31 stations.

One set of KMS Technologies MT system was deployed in the morning and left overnight to record the electric and magnetic fields. The equipment was recovered and moved to the next site the next day. To improve the data quality, the MT data was acquired simultaneously from another MT system 600 km south of the study area in Kanchanaburi province where it was treated as a remote reference site. The acquired data around the PFZ was processed with the data at the remote reference site based on the robust multiple-station technique of Egbert (1997). After the data processing, the impedance tensor **Z** and the vertical magnetic transfer function **T** were logarithmically chosen to cover16 periods starting from 1000 Hz to about 600 s, for each site. Some selected apparent resistivities and phases of the *xy*- and *yx*-modes with the error bars are shown in Fig. 3 and the vertical magnetic

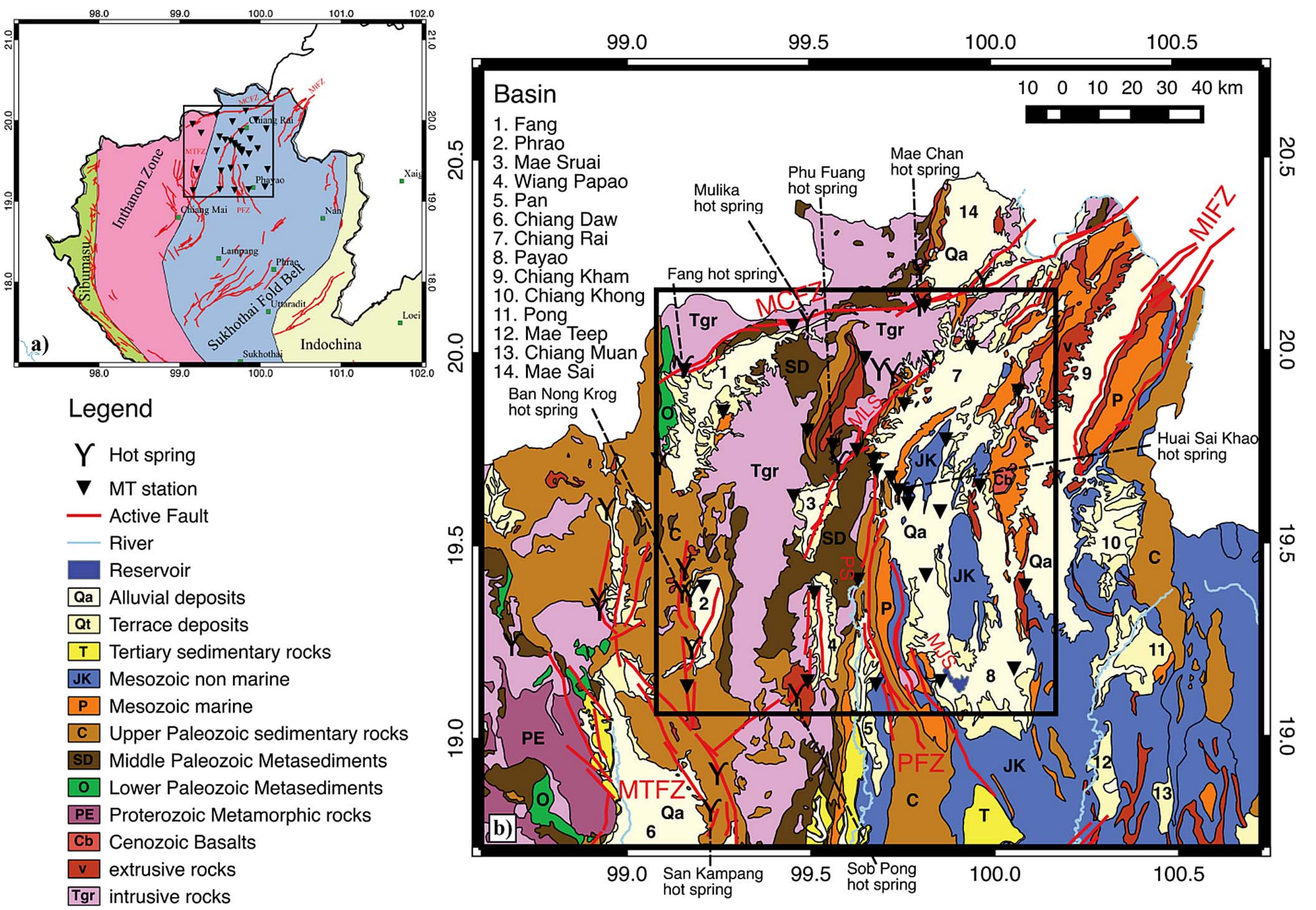


**Fig. 2.** (a) Tectonic setting of northern Thailand (after Metcalfe, 2013). (b) Regional geology covering the area of the study (rectangular block). The triangles are the locations of the MT stations.

transfer functions or tippers in Fig. 4.

The off-diagonal **Z** (Zxy and Zyx) and the tipper **T** from these 31 sites were inverted with the WSINV3DMT parallel version (Siripunvaraporn et al., 2005; Siripunvaraporn and Egbert, 2009). The minimum error floors for both data sets were set at 5%. Several inversions were started from the homogeneous earth with 1–1000 Ω m. All of these initial models were discretized using a 52 × 52 × 44 grid (with 7-air layers on top of the topography) in the north-south, west-east and vertical directions, respectively. The horizontal grid spacing of 4 km in the study area were discretized on average in both directions. Outside of the study area, the horizontal grid spacing was increased in a logarithmic scale to avoid the boundary effects from the forward modeling routine (Siripunvaraporn et al., 2002). The first layer in the vertical direction was finely discretized to provide high accuracy solutions for all periods. The thickness of a given layer was 1.2–2.0 times that of the previous layer.

Most of the inversions starting from different initial models can reduce the RMS misfit from around 15 to within an acceptable level of around 2. Most of the final inverted models show similar resistive and conductive anomalies at the same locations but in some cases of different sizes and depths. However, inverted models starting from low and high resistivity values often produce rough models which over-fit the observed data and are therefore discarded. In addition to the RMS misfit, another constrain to select the final inverted model is basically that it should produce some agreements with the surface geology. Based on these two conditions, the final inverted model was selected from the 300 Ω m initial model after 6 iterations with an RMS of 1.97 and is shown in Figs. 5–7. The correspondence with the surface geology is described in the next section. The 30 hypocenters obtained from Noisagool et al. (2016) for earthquakes with Mw > 3.5 are also plotted in Figs. 5 and 6.

There are many interesting anomalies listed and described in the next section. As in Amatyakul et al. (2016), we performed sensitivity analysis to verify their existence. By replacing the resistivity of the anomaly with the background resistivity (around 100–300 Ω m), implying that this anomaly does not exist, we then run the forward modeling routine and re-compute the misfit of each station. The relative change of the RMS values of each station is computed via, Relative Change = 100% × ($RMS_{new}$ − $RMS_{original}$)/$RMS_{original}$, where $RMS_{new}$ is the fit after replacing the anomaly with the background resistivity, and $RMS_{original}$ is from the inverted model in Figs. 5–7. Relative changes from two interesting anomalies (ML and Qa), as examples, are shown in Fig. 8. By replacing the anomalies with the background, MT stations located near the anomalies show significant changes. This means that these anomalies are required by the observed data and are not the artifacts from over-fitting the data.

## 4. Interpretation and discussion

As stated earlier, there are two main reasons why we prefer the inverted model in Figs. 5 and 6 as our final model. First, it can produce the responses that fit the observed data with an RMS of 1.97 (Fig. 3 and Fig. 4). Second, the surface geology (Fig. 7a) corresponds closely with the final inverted model at 50 m depth (Fig. 7b). West of the PFZ, the Triassic granite rock (Tgr) corresponds well with high resistivity bodies (> 100 Ω m). Most of the Quaternary alluvial deposit (Qa; Fig. 7a) within the study area is imaged as the high conductivity bodies (< 30 Ω m; Fig. 7b). On the east, the Mesozoic non marine (JK) is

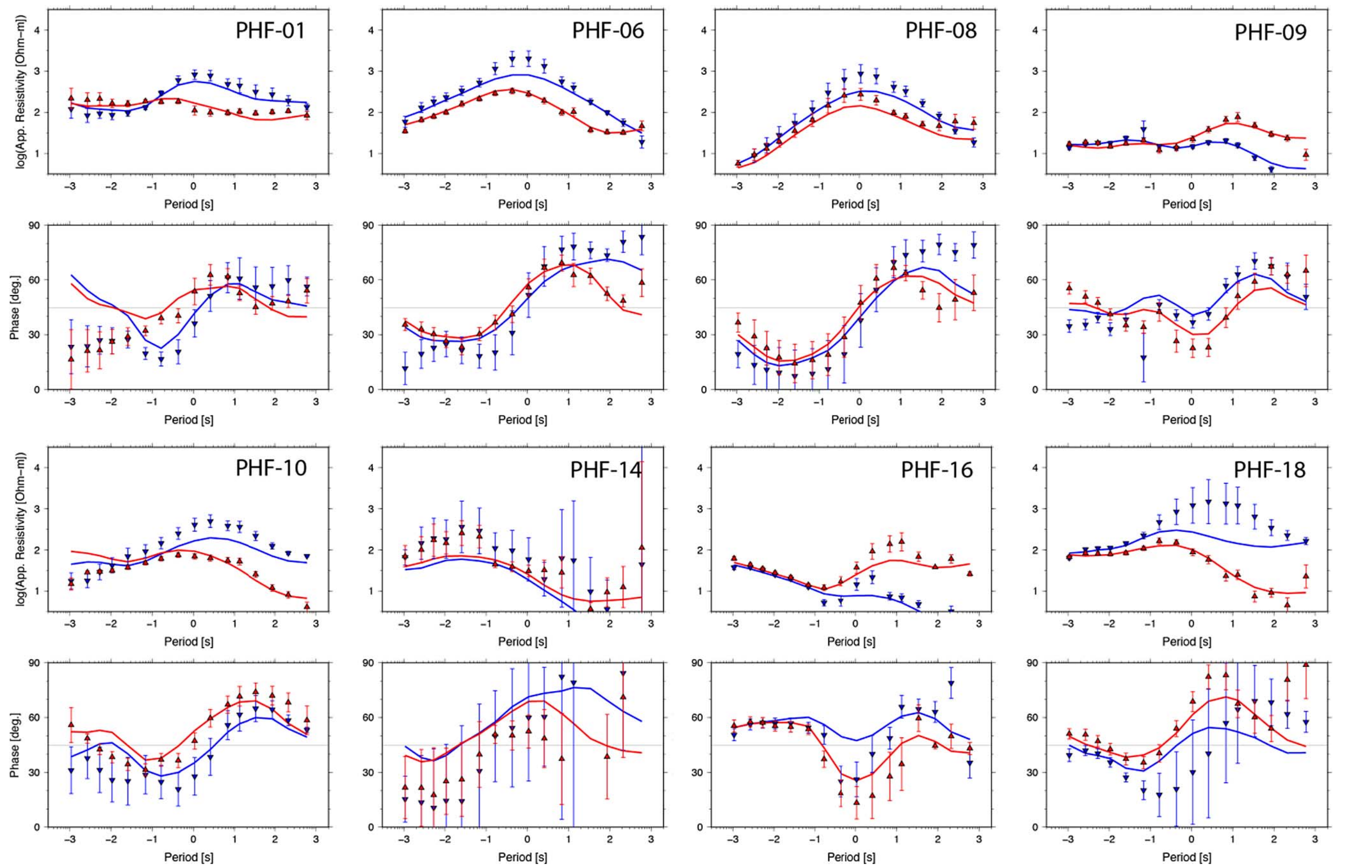


**Fig. 3.** Selected apparent resistivities (Ω m) and phases (in degrees) as a function of $\log_{10}$ periods (seconds) computed from the off-diagonal impedance tensor at various locations acquired in the locations marked as blue crosses in Fig. 2. Red is xy and blue is yx mode. The upward and downward triangles and error bars are from field measurements, and the solid lines are the calculated responses generated from the inverted model shown in Fig. 5. (For interpretation of the references to color in this figure legend, the reader is referred to the web version of this article.)

scattered around the Qa (Fig. 7a). The JK is mapped as the high resistivity body. Within the PFZ at this depth, the Silurian/Devonian meta-sediments (SD) and volcanic rocks are seen as a moderate resistivity (≈100 Ω m).

### *4.1. Correspondence of the shallow conductors to the hot springs at surface, and to the basins*

Locations of many hot springs in our study area have already been shown in Fig. 2. However, since many readers may not be familiar with the local geography, in this section, we also plot the locations and the labels on Figs. 6a and 7b. On the west and north of the PFZ, even though there is a large resistive region (T; Figs. 5, 6 and 7b) which dominates from the surface to a depth of around 20 km, there are still many conductive anomalies within the resistive T zone. In the north of the study area, near the Fang hot spring (Fig. 6a), the conductive F anomaly (Fig. 6a and b) can be mapped to about 2–3 km depth. This F conductive zone with similar thickness was also seen in the earlier MT geothermal survey using more closely spaced MT stations (Amatyakul et al., 2016) and was interpreted as the sedimentary rock of the Fang basin. The F anomaly here is therefore likely to represent the Fang basin, also confirming a study of Sethakul and Pimasarn (1990) which estimated the Fang basin to be about 3 km thick (Morley et al., 2011).

About 40 km to the east of the F anomaly and to the north of the study area, there is another large conductive zone (MCH) occurring slightly south of the Mae Chan Fault Zone (MCFZ) located in between the famous Mae Chan hot spring and Mulika hot spring in the west (Figs. 2b, 6a and 7b). This MCH conductor extends to a depth of 3 km before being replaced by the resistive body. This MCH conductor did not appear in our previous MT survey (Amatyakul et al., 2015) as the earlier study was focused just around a few square kilometers of the Mae Chan hot spring. It is therefore very interesting to have this high conductivity body in the region dominated by the Triassic granite at the surface which was interpreted as the heat source of the Mae Chan hot spring (Amatyakul et al., 2015). To determine whether this MCH conductor plays any roles with the MCFZ or acts as the hot reservoir serving the two hot springs, more geophysical and geological studies should be conducted to probe this conductive feature.

In the vicinity of the PFZ, there are two large and shallow conductors (PF1 and PF2; Figs. 6a and b and 5c) located next to the Phu Faung hot spring (Figs. 2b and 6a). PF1 (Fig. 6a) is very shallow and south of the hot spring, whereas PF2 (Fig. 6b) is deeper and north of the hot spring. At this point, we do not know whether PF1 and PF2 are connected. Further closely spaced MT sites around the region are necessary to probe the connection. As PF1 and PF2 are closer to the hot spring and have similar thickness and depth to the fluid reservoir of the Fang hot spring (see Amatyakul et al., 2016), it is possible that both are involved with the Phu Faung hot spring, or just the Silurian/Devonian meta-sediments with high water content as found in the surface. In contrast to the MCH, F, PF1 and PF2 conductors found beneath the other hot springs, there is no conductor found beneath the Huai Sai Khao hot spring (Figs. 2b and 6a). In between the Mae Lao Segment (MLS) and the Pan segment (PS), there is an S conductor located around 500–3 km depth (Fig. 6b). Unlike other conductors (F, PF1 & PF2 and MCH), the location of this S conductor cannot be linked to any of the hot springs. This might be one piece of evidence to indicate that this kind of conductor is not necessarily associated with the hot springs, and vice versa for the case of the Huai Sai Khao hot spring.

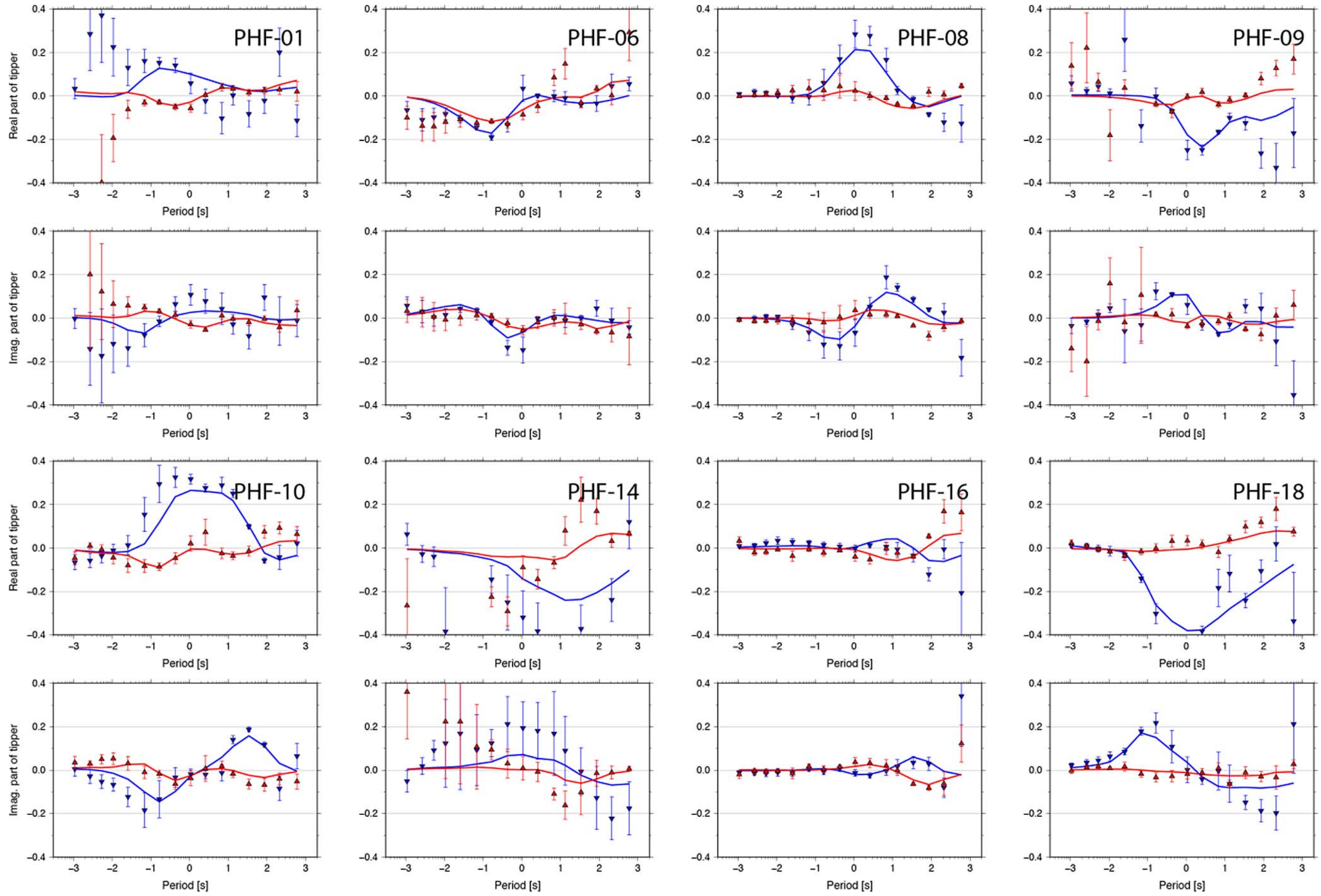


**Fig. 4.** Real and imaginary parts of the vertical magnetic transfer functions (tipper) as a function of $\log_{10}$ periods (seconds) at various locations acquired in the locations marked as blue crosses in Fig. 2. Red is zx and blue is zy mode. The upward and downward triangles and error bars are from field measurements, and the solid lines are the calculated responses generated from the inverted model shown in Fig. 5. (For interpretation of the references to color in this figure legend, the reader is referred to the web version of this article.)

On the east of the PFZ, the Quaternary alluvial deposit (Qa; Fig. 7) mapped at the surface as the conductive body, appears to be less than 1 km thick (Fig. 7a and b) which is thinner than the basin on the west and north of the PFZ. The alluvial deposit is overlain on a resistive body (J; Fig. 6a and b) where at the surface the J is in agreement with the Mesozoic non marine (JK; Figs. 2b and 7a). The J resistor remains to about 3 km depth, which might be a typical thickness of the Mesozoic non marine sedimentary rock, before being replaced with the moderate resistivity layer. Near the eastern edge of the study, there is another resistive body at a depth greater than 4 km (Fig. 6c). We are not certain whether this resistive body is the continuation of the J resistor going deeper to the east or a different anomaly since we have limited data.

### *4.2. Mid to lower crust conductive and resistive anomalies of and around the PFZ*

There are many interesting conductive and resistive features located both in between the Mae Lao segment (MLS) and the Pan segment (PS) of the PFZ (Figs. 2b and 6a), and along the sides of the PFZ. In the upper to middle crust, Figs. 5 and 6 clearly show that the PFZ cuts into the resistive zones: the resistive (T; Figs. 5b–f and 6a–e) zone on the west of the MLS, and another narrow resistive band (R1; Figs. 5d–f and 6b–d) located in between the PS and the Mae Jai Segment (MJS). Based on the geology map (Figs. 2b and 7a), the Triassic granite is observed on the west of the MLS and corresponds well with the T resistive zone. Both features can then be conveniently linked together, similar to what we found in the Fang geothermal study (Amatyakul et al., 2016) and in the Mae Chan geothermal study (Amatyakul et al., 2015) where the high resistive zone was linked to the Triassic granite.

In contrast to the west, granite is rarely found on the surface on the east of the PS (Figs. 2b and 7a), as the area is mostly overlain by the alluvial deposits and the meta-sediments (Fig. 2b) at the surface. It is interesting to observe that the narrow resistive R1 zone that appears in between the PS and the MJS has about the same depth as the T resistive zone (Fig. 5d–f). We therefore identify the R1 as the batholith granite, similar to the T resistive zone. If R1 and T are the same granite belt, it indicates that the PFZ has separated the intrusive granite rocks into two zones, where R1 is in the eastern edge of the rock and T is on the west. If not the same type, it indicates that R1 had slipped from the north to attach here. Another interesting resistive anomaly is R2 (Figs. 6d–f and 5b–c, g and h). R2 does not appear until below 10 km. Its appearance coincidently marks the termination of the PS segment. Its role is also very important for the seismicity of the 5 May 2014 event and aftershock as most of the seismicity occurred above it (Fig. 6d). Similarly, R2 and the T and R1 resistive zones can be interpreted as the S-type biotite granites that originated during the collision of the Sibumasu and Indochina terranes during the mid-Triassic.

In between the MLS and PS faults, there is an ML conductor (Figs. 5d and g, and 6c–e) near the center of the study area, and the P2 conductor (Figs. 5f and h, and 6c–f) in the south of study area. The Mae Lao segment just runs through this ML conductive anomaly which is why we named it ML. The location of ML is almost identical to the very shallow PF1 (Fig. 6a) and near the Phu Faung hot spring (Fig. 6a). As the ML conductor has a depth from about 4 km to the lower crust (Fig. 5f), its relationship with the hot spring is uncertain. At about the same depth, most of the epicenters occurred just north of the ML conductor. This indicates that the ML conductor might play an important role in the earthquake sequence of the 5 May 2014 event occurring on both MLS

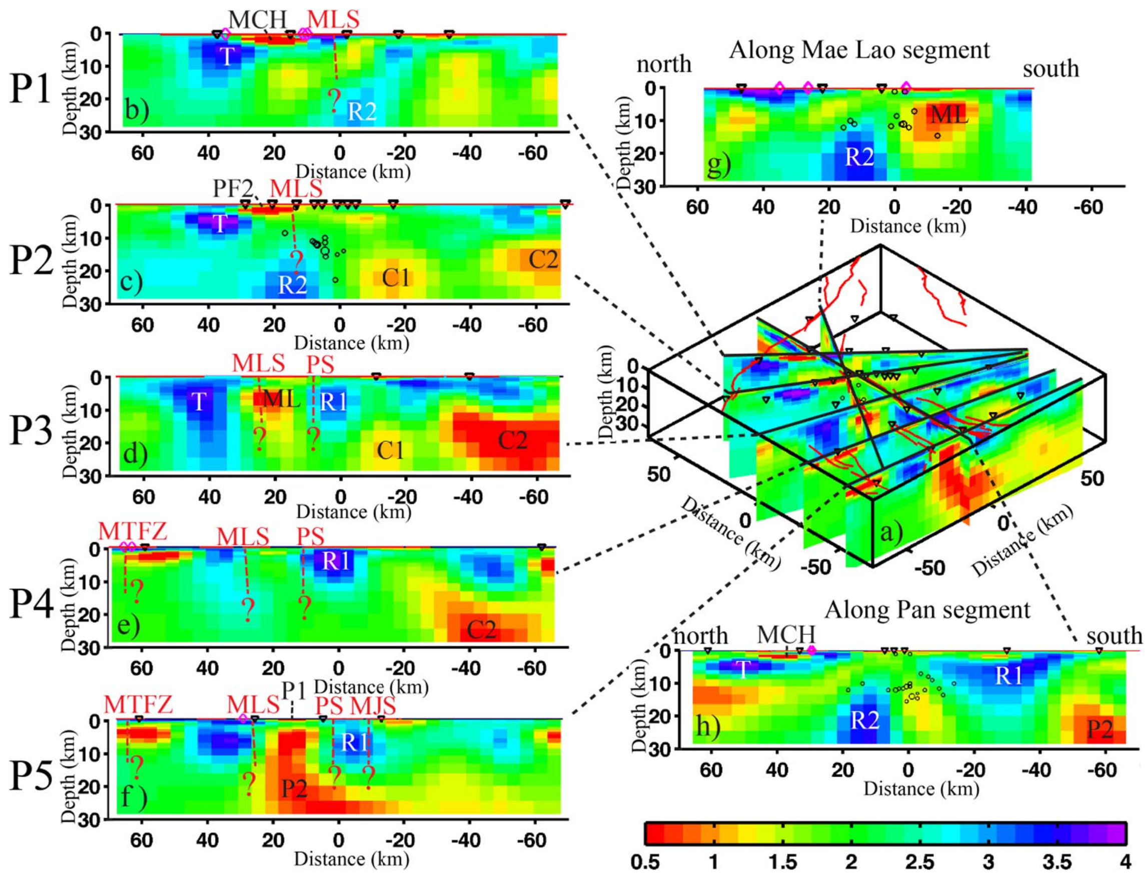


**Fig. 5.** The final inverted model and their cross sections. Epicenters (Noisagool et al., 2016) were projected with 10 km bins (5 km each side of the profile). The color bar is the $\log_{10}$ resistivity in Ω m. (For interpretation of the references to colour in this figure legend, the reader is referred to the web version of this article.)

and PS.

### 4.3. Seismicity and the resistivity anomalies

Based on the recent calculation from the regional waveforms (Noisagool et al., 2016), most of the seismicity on 5 May 2014 (Mw > 3.5) occurred in the seismogenic zone, above a depth of 15 km. As large earthquakes often occur at the highest strength of the brittle crust (Tse and Rice, 1986; Scholz, 1988), the hypocenter depth of the main shock estimated by Noisagool et al. (2016) is therefore reasonable and in agreement with the estimated brittle – ductile transition of Morley et al. (2011) at the depth around 12 km. The inverted model at the depth of 12 km (Fig. 6d) reveals that the seismicity lies mostly around the edge of the ML conductor at the transition zone of the PS and the MLS. Fig. 5g, which displays the cross sectional plot along the MLS segment from north to south, shows that the seismicity is localized around the region of moderate resistivity (around 100 Ω m), above the R2 resistor, but not inside the ML conductor. Similarly, a cross sectional plot from north to south along the PS segment (Fig. 5h) also shows similar patterns; the seismicity just lies above the lower resistive anomaly which might be an extension of the ML conductor to the west, and along the edge of the R1 resistor. The seismicity along the edges of the resistors and conductors were also observed in numerous publications (e.g., Mitsuhata et al., 2001; Ogawa et al., 2001; Ogawa and Honkura, 2004; Ichihara et al., 2011; Bertrand et al., 2012; Unsworth and Bedrosian, 2004a; Rawat et al., 2014; Wannamaker et al., 2014).

As described earlier, there are at least three major possible interpretations to explain the high conductivity around the fault zones in the mid-crust: saline fluid, graphite, and partial melt. It is not easy to pinpoint the cause of the low resistivity ML around the PFZ as we have very limited geological and geophysical information on the area. Although northern Thailand is currently experienced an east – west extension (Morley, 2001, 2007; Simons et al., 2007; Charusiri and Pum-Im, 2009), the temperature of the hot springs around the PFZ is not high enough. The Huai Sai Khao hot spring has a temperature of just around 56 °C at the surface. A partial melt at the upper and mid-crust for the ML conductor is therefore very unlikely. Although graphite was reported to be found in the Fang district, there is no graphite mining in the region. It is therefore unlikely that graphite or other high conductivity ores are a major source for the high conductivity ML.

Here, the aqueous fluid explanation seems to be the most suitable hypothesis for the cause of the earthquakes in this region. This is similar to other publications which often give the high conductivity found to the saline fluid as a possible cause for the seismicity in the region (e.g., Mitsuhata et al., 2001; Bedrosian et al., 2004; Ogawa and Honkura, 2004; Ichihara et al., 2009; Becken and Ritter, 2012; Unsworth and Bedrosian, 2004a, 2004b). The role of high pressure fluid in causing the seismicity has been widely studied (e.g., Tullis et al., 1996; Cox, 2002; Fujimoto et al., 2002). The saline fluid that is trapped and stored within the ML conductor aids in reducing the strength of the faults, particularly the MLS as this segment is richer in fluid than other segments, by lowering the effective normal stress. The high pore fluid pressure in the MLS segment (found from this study) and the higher shear stress from its own geometry (Noisagool et al., 2016) make the fault mechanically weak. The continuous pre-existing tectonic stress coming from the north (Tingay et al., 2010) to northern Thailand (Noisagool et al., 2016) has become larger than the maximum strength that the fault can withstand. The result was that the MLS slipped producing the main shock of 5 May 2014 followed by many aftershocks (Mw > 3.5) occurring between the MLS and PS just within a localized zone of moderate resistivity (around 100 Ω m between the ML conductor and the R2 resistor; Figs. 5c, g and h; and 6d), not directly within the ML conductor

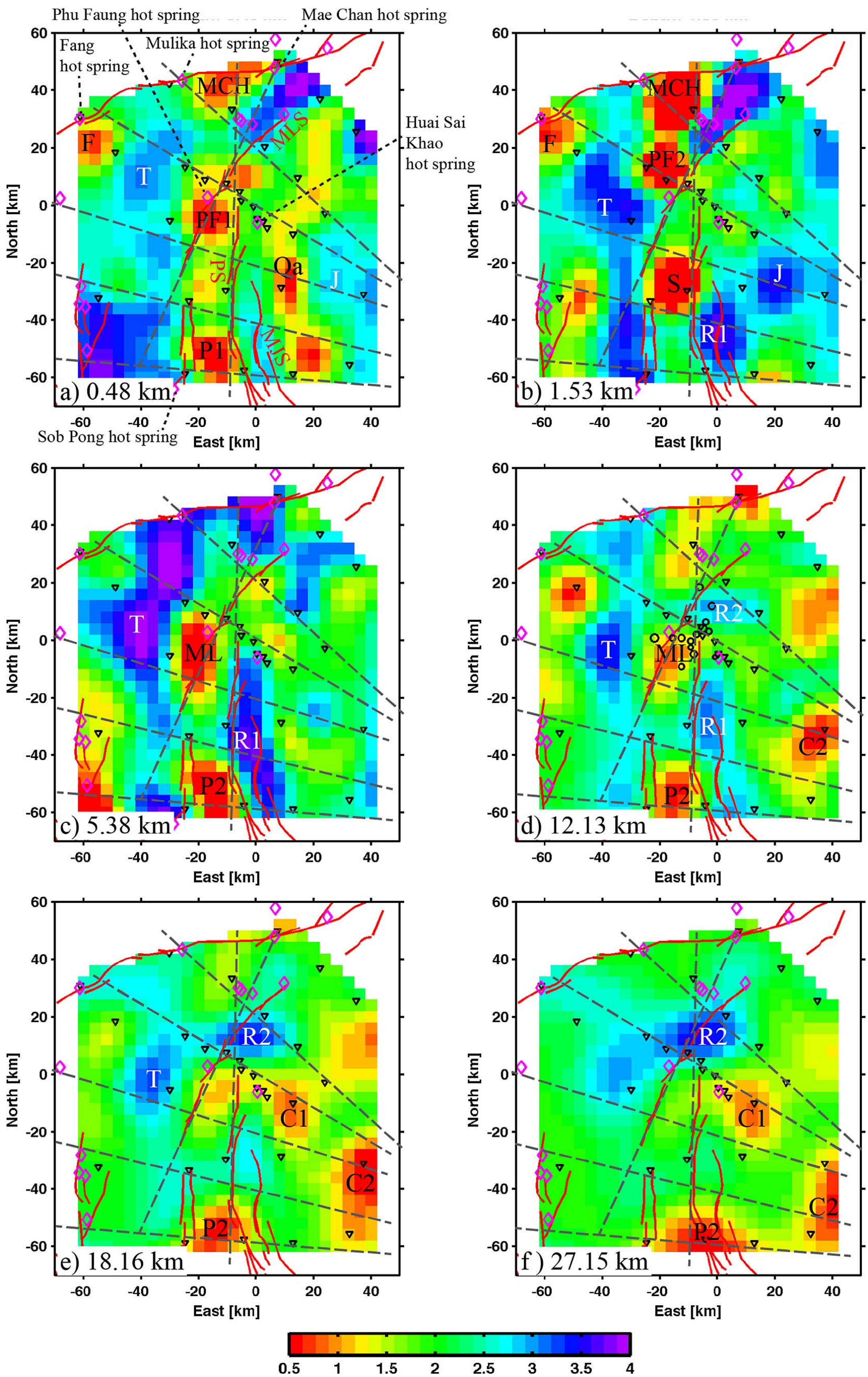


**Fig. 6.** Top view of the final inverted model (Fig. 5) at various depths: (a) 0.5 km, (b) 1.5 km, (c) 5.4 km, (d) 12.1 km, (e) 18.1 km and (f) 27.1 km. MT locations are marked as black triangles, hot springs are pink diamonds. Dashed lines indicate the locations of the cross section in Fig. 5. The color bar is the $\log_{10}$ resistivity in Ω m. (For interpretation of the references to color in this figure legend, the reader is referred to the web version of this article.)

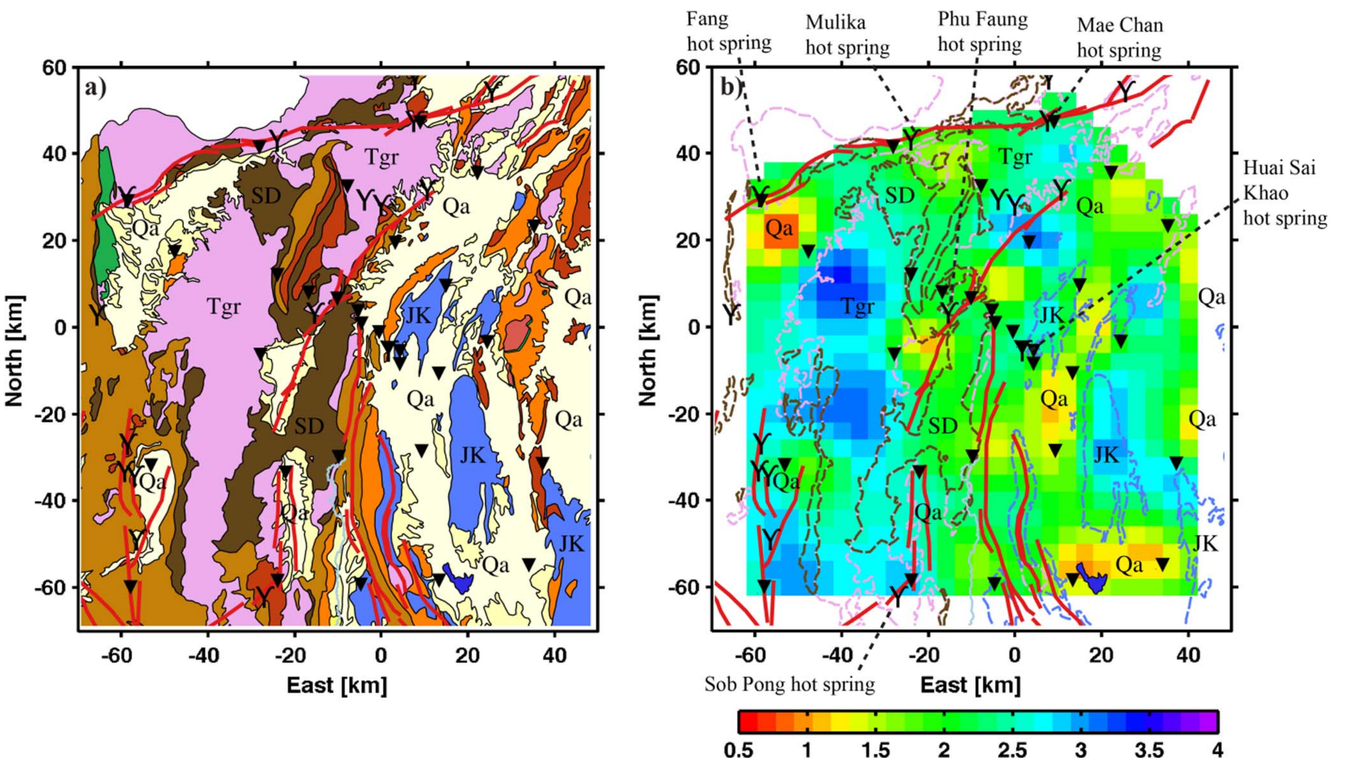


**Fig. 7.** A comparison of (a) the surface geology with (b) a 50 m depth slice of the final inverted model (Fig. 5). The color bar is the $\log_{10}$ resistivity in Ω m. (For interpretation of the references to colour in this figure legend, the reader is referred to the web version of this article.)

nor inside the resistor R2 for both the PS and MLS. This is summarized in the diagram shown in Fig. 9.

Directly above the ML conductor is the PF1 and slightly north is the PF2. In between the PF1 and PF2 conductors and the ML conductor is a thick moderate resistivity layer (about 4 km thick) as shown in Fig. 5g. It is therefore unclear whether PF1 and PF2 have any direct connection to the ML as the magnetotelluric resolutions might not be detailed enough to validate this. However, as the fault cuts through the middle of both conductors, a connection might exist within the MLS segment. If there is a connection, it might indicate that the hot fluid of the Phu Faung hot spring (Figs. 2b and 7b) comes from the deep ML conductor by rising through the fractured granite pathways of the MLS and getting stored in the shallow PF1 and PF2 conductors. We suspect that this is how the high pressure fluid of the ML conductor releases the pressure to

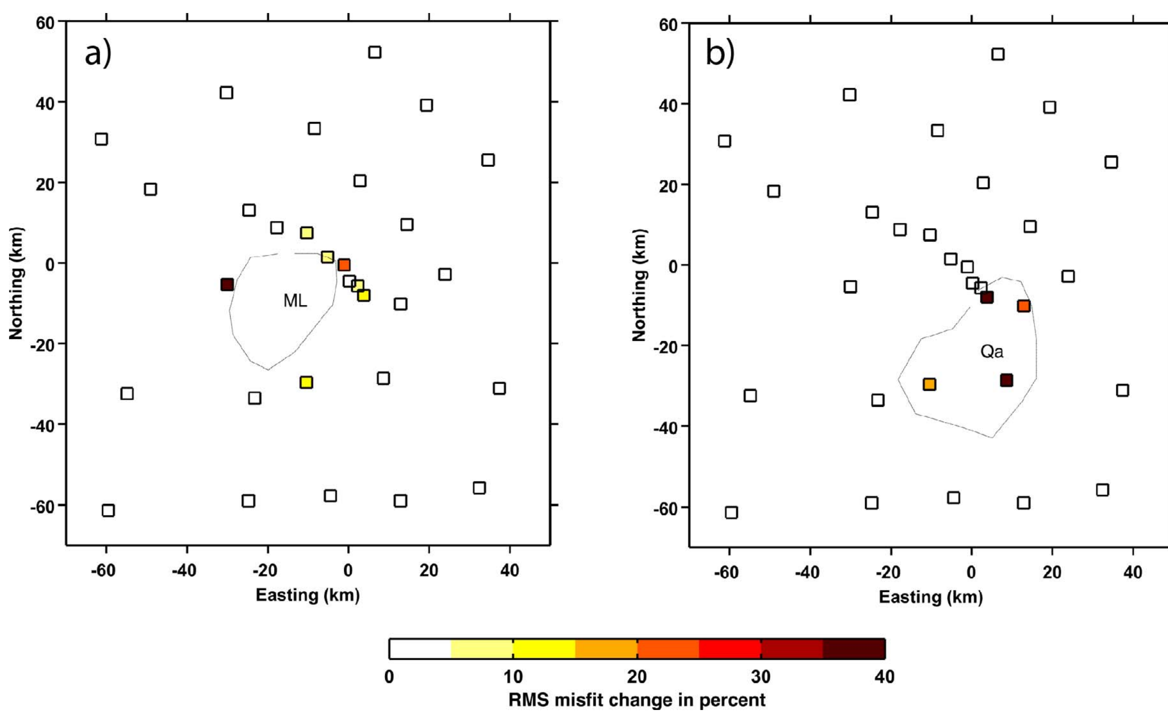


**Fig. 8.** Plots of relative change of RMS misfit of each station in percent (a) after replacing the ML conductor of the inverted model (Figs. 5–7) with the background resistivity, and (b) after replacing Qa conductor with the background resistivity.

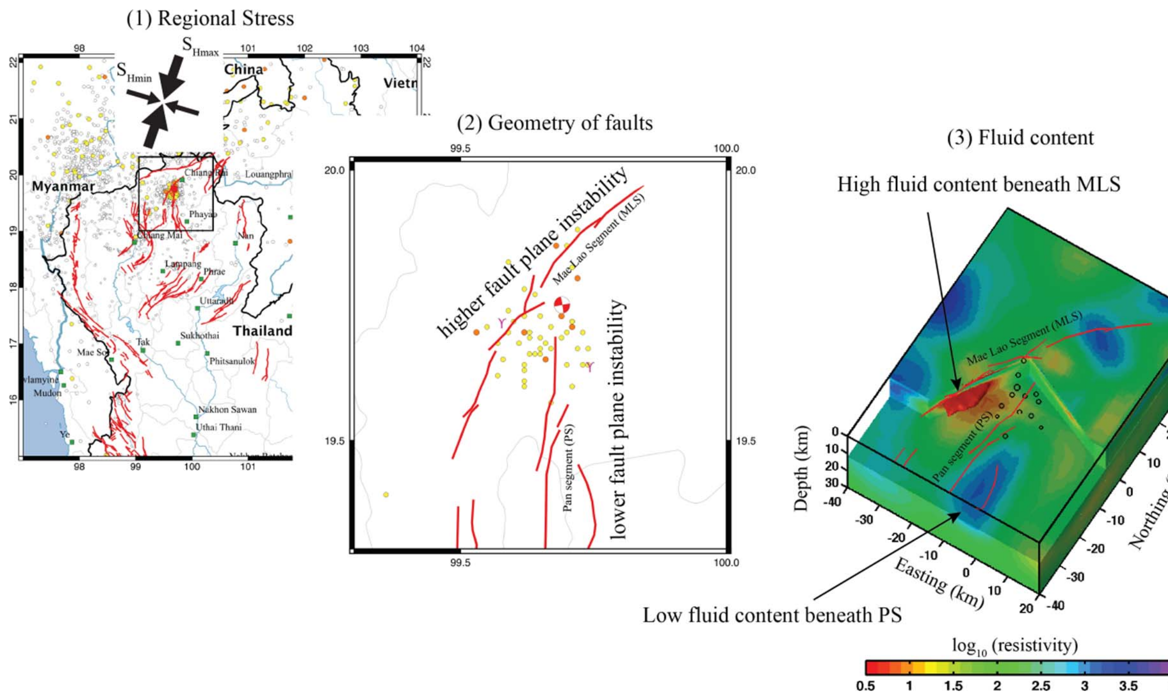


**Fig. 9.** A diagram explaining a hypothesis about the cause of the 5 May 2014 main shock. (1) A pre-existing tectonic stress is continuously being exerted to the northern Thailand region. (2) The Mae Lao Segment (MLS) and the Pan Segment (PS) have different geometry resulting in a higher fault plane instability for the MLS, and lower fault plane instability for the PS. (3) High fluid content from the low resistivity zone is found next to the MLS, but not the PS. The combination of (2) and (3) on the MLS helps to lower the maximum frictional strength of the MLS fault. This makes the MLS fault weaker relative to that of the PS. When accumulated tectonic stress (1) becomes large, it will make the MLS slip first and so produce the main shock.

the environment without causing large earthquakes. Occasionally, when the high pressure becomes large enough, it causes the fault to suddenly slip causing the earthquakes as a way to release the high pressure. Several of the aftershock focal mechanisms indicate all kinds of motions: strike-slip, normal, and thrust motions. The mixed focal mechanisms might be induced by the presence of the fluid in the fault zone. Although we prefer the fluid explanation for the ML conductor, to fully confirm the existence of the fluid, other geophysical techniques are necessary. These include observing the S-wave reflector as in Mitsuhata et al. (2001), Umino et al. (2002) and Aoki et al. (2016), or the Poisson's ratio and the low-Vp and low-Vs features (Zhao et al., 1996, 2004; Mishra and Zhao, 2003; Lei and Zhao, 2009; Mahesh et al., 2012; Wang et al., 2013) or the low density zone (Ichihara et al., 2009).

In the south, there is a large P2 conductor extending from about a depth of 5 km to the 32 km depth Moho and to the mantle (Figs. 5f and Fig. 6c–f). The P2 conductor covers a large area but is mostly within the PFZ. There is also a P1 conductor at a shallow depth above the P2. Nearby P1 is a Sob Pong hot spring. It might therefore be interpreted in a similar way to the other conductors as the resistivity is lowered by the aqueous fluid. The hot fluid of P2 can rise through the many fault segments and get stored in P1, as with the Phu Faung geothermal system in the north. Nevertheless, the difference is there is no seismicity in the region near the P1 and P2 conductors as in the ML conductor. There are many possible reasons to explain the lack of the seismicity in this area. The P1 and P2 conductors are not really fluid related but just conductive rocks. Another possibility is that the geometry of the fault segments in the south is mostly north–south trending. As indicated in the Mohr's diagram of Noisagool et al. (2016), this geometry requires much greater stress from the north to slip than that of the MLS lying in the NE – SW direction. It is therefore more difficult to slip even with the fluid localized in the faults as in the MLS segment. The bottom of the P2 conductor is not well defined as it extends deep into the mantle. As there are not many MT sites in the region near the P2 conductor, we might need more MT measurements in this area to verify the existence of the P1 and P2 conductors and determine their size and depth. As with the ML conductor, other geophysical techniques, particularly the seismic tomography, are necessary.

To the north of the study area, our resistivity structure (Figs. 5 and 6) shows that there is no clear large conductor within the seismogenic zone beneath the Mae Chan Fault Zone (MCFZ). The lack of the large conductor beneath the MCFZ could be one explanation for the lack of the moderate to large seismicity generated by the MCFZ. Without the fluid (as is presented beneath the MLS fault) the MCFZ would require a larger amount of stress in order to slip. Paleo-seismicity (Charusiri et al., 2000; Fenton et al., 2003) has indicated that several large earthquakes have occurred on the MCFZ. Nevertheless, our MT station coverage for this work is mostly in the PFZ region. To further confirm the non-existence of the highly conductive zone within the MCFZ in the upper to mid-crust, more MT stations across the MCFZ would be necessary. Geodetic measurement for the slip rate in the area might also be necessary to assess the present-day motions of the faults in the northern Thailand.

Figs. 5 and 6 shows the existence of the deeper conductors, C1 and C2 on the eastern side of the PFZ in the lower crust below the estimated brittle – ductile transition (Morley et al., 2011). Although the presence of C1 and C2 are beyond the scope of the current study, they both might be related to the crustal extension in northern Thailand (Morley, 2001, 2007; Simons et al., 2007; Charusiri and Pum-Im, 2009;) and both conductors might be dehydrated metamorphic rocks in the lower crust (Hyndman and Shearer, 1989) or fluids released from the magma (Abdul Azeez et al., 2013). They could also be remnant dehydration fluid accumulated during the Permo-Triassic subduction like what lies beneath Kanchanaburi province, western Thailand (Boonchaisuk et al., 2013). However, both hypotheses require further investigation via other geological and geophysical techniques.

## 5. Conclusion

- A total of 31 magnetotelluric (MT) stations were deployed within a 140 km × 140 km area to investigate the Phayao Fault Zone (PFZ) rupture area in northern Thailand.
- We found conductive anomalies beneath the Mae Lao Segment

(MLS) and partially beneath the Pan Segment (PS) from a depth of 4 km to mid-crust where both MLS and PS are part of the PFZ. They were interpreted as saline fluid rich zones.
- The saline fluid rich zones strongly support our assumption of previous studies (Noisagool et al., 2016) that the MLS is the slipping fault producing the main event of 5 May 2014. The energy was then transferred to the PS resulting in slipping in both the MLS and PS causing the aftershocks.

## Acknowledgement

This research has been supported by the Development and Promotion of Science and Technology Research Grant 037/2557, the Thailand Center of Excellence in Physics (ThEP), and the Thailand Research Fund (RSA5780010). We would like to thank Dr. Michael Allen for editing the English of this manuscript, and the two reviewers who provide many good comments to improve the manuscript.

## References

Abdul Azeez, K.K., Unsworth, M.J., Patro, P.K., Harinarayana, T., Sastry, R.S., 2013. Resistivity structure of the Central Indian Tectonic Zone (CITZ) from Multiple Magnetotelluric (MT) profiles and tectonic implications. Pure Appl. Geophys. 170, 2231–2256.

Aoki, S., Iio, Y., Katao, H., Miura, T., Yoneda, I., Masayo, S., 2016. Three-dimensional distribution of S wave reflectors in the northern Kinki district, southwestern Japan, Earth. Planets Space 68, 107.

Amatyakul, P., Rung-Arunwan, T., Siripunvaraporn, W., 2015. A pilot magnetotelluric survey for geothermal exploration in Mae Chan region, northern Thailand. Geothermics 55, 31–38.

Amatyakul, P., Boonchaisuk, S., Rung-Arunwan, T., Vachiratienchai, C., Wood, S.H., Pararai, K., Fuangswasdi, A., Siripunvaraporn, W., 2016. Exploring the shallow geothermal fluid reservoir of Fang geothermal system, Thailand via a 3-D magnetotelluric survey. Geothermics 64, 516–526.

Becken, M., Ritter, O., 2012. Magnetotelluric studies at the San Andreas fault Zone: implications for the role of fluids. Surv. Geophys. 33, 65–105.

Bedrosian, P.A., Unsworth, M.J., Egbert, G., 2002. Magnetotelluric imaging of the creeping segment of the San Andreas Fault near Hollister. Geophys. Res. Lett. 29, 1–4.

Bedrosian, P.A., Unsworth, M.J., Egbert, G., Thurber, C.H., 2004. Geophysical images of the creeping segment of the San Andreas fault: implications for the role of crustal fluids in the earthquake process. Tectonophysics 385, 137–158.

Bertrand, E.A., Unsworth, M.J., Chiang, C.-W., Chen, C.-S., Chen, C.-C., Wu, F.T., Türkoğlu, E., Hsu, H.-L., Hill, G.J., 2012. Magnetotelluric imaging beneath the Taiwan orogen: an arc-continent collision. J. Geophys. Res. 117, B01402.

Boonchaisuk, S., Siripunvaraporn, W., Ogawa, Y., 2013. Evidence for middle Triassic to Miocene dual subduction zones beneath the Shan-Thai terrane, western Thailand from magnetotelluric data. Gondwana Res. 23, 1607–1616.

Charusiri, P., Clark, A.H., Farrad, E., Archibald, D., Charusiri, B., 1993. Granite belts in Thailand: evidence from the 40Ar/39Ar geochronological and geological syntheses. J. SE Asian Earth Sci. 8, 127–136.

Charusiri, P., Kosuwan, S., Lumjuan, A., Wechbunthung, B., 1999. Review of active faults and seismicity in Thailand. GEOSEA'98. Bull. Geol. Soc. Malays. 43, 653–655.

Charusiri, P., Kosuwan, S., Daorerk, W., Wechbunthung, B., Kuthranon, S., 2000. Earthquake in Thailand and Southeast Asia Mainlan, Complete Report (in Thai), Thailand Research Fund. 212 pp.

Charusiri, P., Pum-Im, S., 2009. Cenozoic tectonic evolution of major sedimentary Basins in Central, Northern, and the Gulf of Thailand. Bull. Earth Sci. Technol. 2, 40–62.

Cox, F., 2002. Fluid flow in mid-to deep crustal shear systems: experimental constraints, observations on exhumed high fluid flux shear systems, and implications for seismogenic processes. Earth, Planets and Space 54, 1121–1125.

Department of Mineral Resource, 2007. Geology and Resource Chiang Rai Province Classification and Management. Department of Mineral Resource, Thailand (in Thai).

Department of Mineral Resource, 2014. Report on a Study of 5th May 2014, 6.3 Earthquake. Department of Mineral Resource, Thailand (in Thai).

Egbert, G.D., 1997. Robust multiple-station magnetotelluric data processing. Geophys. J. Int. 130, 475–496.

Fenton, C.H., Charusiri, P., Wood, S.H., 2003. Recent paleoseismic investigations in Northern and Western Thailand. Ann. Geophys. 46, 957–981.

Fujimoto, K., Ohtani, T., Shigematsu, N., Miyashita, Y., Tomita, T., Tanaka, H., Omura, K., Kobayashi, Y., 2002. Water-rock interaction observed in the brittle-plastic transition zone. Earth Planets Space 54, 1127–1132.

Hinthong C, 1995. The study of active faults in Thailand. Proceedings of the technical conference on the progression and vision of mineral resources development. Department of Mineral Resources, Bangkok, pp. 129–140.

Hyndman, R.D., Shearer, P.M., 1989. Water in the lower continentalcrust: Modeling magneto-telluric and seismic reflection results. Geophys. J. Int. 98, 343–365.

Ichihara, H., Mogi, T., Hase, H., Watanabe, T., Yamaya, Y., 2009. Resistivity and density modeling in the 1938 Kutcharo earthquake source area along a large caldera boundary. Earth, Planets Space 61, 345–356.

Ichihara, H., Uyeshima, M., Sakanaka, S., Ogawa, T., Mishina, M., Ogawa, Y., Nishitani, T., Yamaya, Y., Watanabe, A., Morita, Y., Yoshimura, R., Usui, Y., 2011. A fault-zone conductor beneath a compressional inversion zone, northeastern Honshu, Japan. Geophys. Res. Lett. 38, L09301.

International Seismological Centre, 2012, On-line Bulletin. Internatl. Seis. Cent., Thatcham, United Kingdom < http://www.isc.ac.uk > .

Kosuwan, S., Charusiri, P., Takashima, I., Lumjuan, A., 1998. Active tectonics of the Mae Chan Fault, northern Thailand. In: Proceedings of the Ninth Regional Conference on Geology, Mineral and Energy Resources of Southeast Asia, Geological Society of Malaysia, Kuala Lumpur, 16–20 August 1998 (extended abstract).

Kosuwan, S., Lumjuan, A., 1999. Neotectonics of the Mae Chan Fault in Mae Chan District, Chiang Rai Province. Technical Report. Geological Survey Division, Department of Mineral Resources, Bangkok, Thailand.

Kosuwan, S., Saithong, P., Lumjuan, A., Takashima, I., Charusiri, P., 2000. Preliminary Results of Paleoseismic Studies on the Mae Ai segment of the Mae Chan Fault Zone, Chiang Mai, Northern Thailand. Proceedings of the International Symposium on Coordinating Committee for Coastal and Offshore Geoscience Programmes in East and Southeast Asian CCOP), Bangkok, P. 17–27.

Kosuwan, S., Saithong, P., Lumjuan. A., 2003. Paleoearthquake on the Mae Ai Segment of the Mae Chan Fault Zone, Chiang Mai, Northern Thailand: Report of Geological Survey Division, Department of Mineral Resources, 57 p. (in Thai with English abstract).

Lei, J., Zhao, D., 2009. Structural heterogeneity of the Longmenshan fault zone and the mechanism of the 2008 Wenchuan earthquake (Ms 8.0). Geochem. Geophys. Geosyst. 10, Q10010.

Mahesh, P., Gupta, S., Rai, S.S., Rajagopala Sarma, P., 2012. Fluid driven earthquakes in the Chamoli Region, Garhwal Himalaya: evidence from local earthquake tomography. Geophys. J. Int. 191, 1295–1304.

Metcalfe, I., 1997. The Palaeo-Tethys and Palaeozoic-Mesozoic tectonic evolution of Southeast Asia. In: Proceedings of The International Conference on Stratigraphy and Tectonic Evolution of Southeastern Asia and the South Pacific (GEOTHAI '97). Department of Mineral Resources, Thailand, pp. 260–272.

Metcalfe, I., 2013. Gondwana dispersion and Asian accretion: tectonic and palaeogeographic evolution of eastern Tethys. J. Asian Earth Sci. 66, 1–33.

Mishra, O.P., Zhao, D., 2003. Crack density, saturation rate and porosity at the 2001 Bhuj, India, earthquake hypocenter: a fluid-driven earthquake? Earth Planet. Sci. Lett. 212, 393–405.

Mitsuhata, Y., Ogawa, Y., Mishina, M., Kono, T., Yokokura, T., Uchida, T., 2001. Electromagnetic heterogeneity of the seismogenic region of 1962 M6.5 northern Miyagi earthquake, northeastern Japan. Geophys. Res. Lett. 28, 4371–4374.

Morley, C.K., 2001. Combined escape tectonics and subduction rollback back-arc extension: a model for the evolution of Cenozoic rift basins in Thailand, Malaysia and Laos. J. Geol. Soc., London 158, 461–474.

Morley, C.K., 2007. Variations in Late Cenozoic-Recent strike-slip and oblique-extensional geometries, within Indochina: the influence of pre-existing fabrics. J. Struct. Geol. 29, 36–58.

Morley, C.K., Charusiri, P., Watkinson, I.M., 2011. Structural geology of Thailand during the Cenozoic. In: Ridd, M.F., Barber, A.J., Crow, M.J. (Eds.), The Geology of Thailand. Geological Society of London, pp. 273–334.

Noisagool, S., Boonchaisuk, S., Pronsopin, P., Siripunvaraporn, W., 2016. The regional moment tensor of the 5 May 2014 Chiang Rai earthquake (Mw = 6.5), Northern Thailand, with its aftershocks and its implication to the stress and the instability of the Phayao Fault Zone. J. Asian Earth Sci. 127, 231–246.

Naganjaneyulu, K., Santosh, M., 2010. The Central India Tectonic Zone: a geophysical perspective on continental amalgamation along a Mesoproterozoic suture. Gondwana Res. 18, 547–564.

Nutalaya, P., Sodsri, S., Arnold, E.P., 1985. Thailand, Series on seismology, Southeast Asia Association of Seismology and Earthquake Engineering, vol. II, pp. 403.

Ogawa, Y., Mishina, M., Goto, T., Satoh, H., Oshiman, N., Kasaya, T., Takahashi, Y., Nisitani, T., Sakanaka, S., Uyeshima, M., Takahashi, Y., Honkura, Y., Matsushima, M., 2001. Magnetotelluric imaging of fluids in intraplate earthquakes zones, NE Japan back arc. Geophys. Res. Lett. 28, 3741–3744.

Ogawa, Y., Honkura, Y., 2004. Mid-crustal electrical conductors and their correlations to seismicity and deformation at Itoigawa-Shizuoka Tectonic Line, Central Japan. Earth, Planets Space 56, 1285–1291.

Patro, P.K., Harinarayana, T., Sastry, R.S., Rao, M., Manoj, C., Naganjaneyulu, K., Sarma, S.V.S., 2005. Electrical imaging of Narmada-Son Lineament Zone, Central India from magnetotellurics. Phys. Earth Planet. Inter. 148, 215–232.

Phodee, P., Trisirisatayawong, I., Aobpaet, A., 2014. Coseismic and postseismic displacement of 2011 Mw 6.8 Tarlay Earthquake, Myanmar using InSAR techniques and inversion analysis. Engineering J. 19, 157–169.

Rao, C.K., Ogawa, Y., Gokarn, S.G., Gupta, G., 2004. Electromagnetic imaging of magma across the Narmada Son lineament, central India. Earth, Planets Space 56, 229–238.

Rawat, G., Arora, B.T., Gupta, P.K., 2014. Electrical resistivity cross-section across the Garhwal Himalaya: proxy to fluid-seismicity linkage. Tectonophysics 637, 68–79.

Rymer, M.J., Weldon II, R.J., Prentice, C.S., Kosuwan, S., Lumjuan, A., Muangnoicharoen, N., 1997. Tectonic setting and Late Quaternary activity along the Mae Chan Fault, Northern Thailand and Western Laos, Geological Society of America, Abstracts with Programs 29, 229–230.

Scholz, C.H., 1988. The critical slip distance for seismic faulting. Nature 336, 761–763.

Sethakul, N., Pimasarn, V., 1990. Source rock screening and oil/source correlation in the IF 30–01G and 30–02S wells, Fang Field, Thailand. In: Proceedings of the Annual Technical Meeting 1989 and IGCP-246 (1991). Department of Geological Sciences, Chiang Mai University, Thailand, pp. 111–140.

Simons, W.J.F., Socquet, A., Vigny, C., Ambrosius, B.A.C., Abu, S.H., Promthong, C., SubaryaSarsito, D.A., Matheussen, S., Morgan, P., Spakman, W., 2007. A decade of GPS in Southeast Asia: resolving Sundaland motion and boundaries. J. Geophys. Res.

112, B06420.
Siripunvaraporn, W., Egbert, G., Lenbury, Y., 2002. Numerical accuracy of magnetotelluric modeling: a comparison of finite difference approximations. Earth, Planets Space 54, 721–725.
Siripunvaraporn, W., Egbert, G., Lenbury, Y., Uyeshima, M., 2005. Three-dimensional Magnetotelluric inversion: data-space method. Phys. Earth Planet. Inter. 150, 3–14.
Siripunvaraporn, W., Egbert, G., 2009. WSINV3DMT: vertical magnetic field transfer function inversion and parallel implementation. Phys. Earth Planet. Inter. 173, 317–329.
Sone, M., Metcalfe, I., 2008. Parallel Tetyan sutures in mainland Southeast Asia: new insights for Palaeo-Tethys closure and implications for the Indosinian Orogeny. C.R. Geosci. 340, 166–179.
Sone, M., Metcalfe, I., Chaodumrong, P., 2012. The Chanthaburi terrane of southeastern Thailand: stratigraphic confirmation as a disrupted segment of the Sukhothai Arc. J. Asian Earth Sci. 61, 16–32.
Tingay, M.R.P., Morley, C.K., Hillis, R.R., Meyer, J., 2010. Present-day stress orientation in Thailand's basins. J. Struct. Geol. 32, 235–248.
Tullis, J., Yund, R.A., Farver, J., 1996. Deformation-enhanced fluid distribution in feldspar aggregates and implicates for ductile shear zones. Geology 24, 63–66.
Tse, S.T., Rice, J.R., 1986. Crustal earthquake instability in relation to the depth variation of frictional slip properties. J. Geophys. Res. 91, 9452–9472.
Unsworth, M.J., Bedrosian, P.A., 2004a. Electrical resistivity structure at the SAFOD site from magnetotelluric exploration. Geophys. Res. Lett. 31, L12S05.
Unsworth, M.J., Bedrosian, P.A., 2004b. On the geoelectric structure of major strike-slip faults and shear zones. Earth, Planets Space 56, 1177–1184.
Umino, N., Ujikawa, H., Hori, S., Hasegawa, A., 2002. Distinct S-wave reflectors (Bright spots) detected beneath the Nagamachi-Rifu fault, NE Japan. Earth, Planets Space 54, 1021–1026.
Uttamo, W., Elders, C., Nichols, G., 2003. Relationships Between Cenozoic Strike-Slip Faulting and Basin Opening in Northern Thailand. Geol. Soc. Spec. Pub. 210, 89–108.
Wang, J., Zhao, D., Yao, Z., 2013. Crustal and uppermost mantle structure and seismotectonics of North China Craton. Tectonophysics 582, 177–187.
Wannamaker, P.E., Jiracek, G.R., Stodt, J.A., Caldwell, G., Gonzalez, V.M., Mcknight, J.D., Porter, A.D., 2002. Fluid generation and pathways beneath an active compressional orogen, the New Zealand Southern Alps, inferred from magnetotelluric data. J. Geophys. Res. 107 ETG 6-1–ETG 6-20.
Wannamaker, P.E., Evans, R.L., Bedrosian, P.A., Unsworth, M.J., Maris, V., McGary, R.S., 2014. Segmentation of plate coupling, fate of subduction fluids, and modes of arc magmatism in Cascadia, inferred from magnetotelluric resistivity. Geochem. Geophys. Geosyst. 15, 4230–4253.
Wood, S.H., 1995. Late Cenozoic faulting in mountainous regions of low but persistant historic seismicity: Hells Canyon (NW U.S.A.) and Northern Thailand and the meaning of active fault, in IUGG XXI General Assembly, Abstracts Week B, B344.
Wood, S.H., 2001. Slip-rate estimate from offset streams, valley volumes, and denudation rate: Mae Chan Fault, Northern Thailand, American Geophysical Union, Fall Meeting 2001, 82, 932.
Wood, S.H., Singharajwarapan, F.S., Bundarnsin, T., Rothwell, E., 2004. Mae Sai Basin and Wiang Nong Lom: radiocarbon dating and relation to the active strike-slip Mae Chan Fault, Northern Thailand. In: Rieb, S., Wongpornchai, P., Chantraprasert, S. (Eds.), Proceedings of the International Conference on Applied Geophysics. Chiang Mai University, Chiang Mai, Thailand, pp. 60–69.
Wood, S.H., Singharajwarapan, F.S., 2014. Geothermal systems of northern Thailand and their association with faults active during the Quaternary. Geothermal Resour. Council Trans. 38, 607–615.
Wood, S.H., Wood, L.R., Ziegler, A.D., 2015. Natural degradation of earthworks, trenches, walls and moats, Northern Thailand. J. Field Archaeol. 40, 675–694.
Zhao, D.P., Kanamori, H., Negishi, H., Wiens, D., 1996. Tomography of the source area of the 1995 Kobe earthquake: evidence for fluids at the hypocenter? Science 274, 1891–1894.
Zhao, D.P., Tani, H., Mishra, O.P., 2004. Crustal heterogeneity in the 2000 western Tottori earthquake region: effect of fluids from slab dehydration. Phys. Earth Planet. Inter. 145, 161–177.